

TRANSMITTER-GROUPING ROBUST CAPON BEAMFORMING FOR BREAST CANCER DETECTION

D. Byrne, M. O'Halloran, E. Jones, and M. Glavin

College of Engineering and Informatics
National University of Ireland Galway
University Road, Galway, Ireland

Abstract—Early detection of tumor tissue is one of the most significant factors in the successful treatment of breast cancer. Microwave breast imaging methods are based on the dielectric contrast between normal and cancerous tissues at microwave frequencies. When the breast is illuminated with a microwave pulse, the dielectric contrast between these tissues can result in reflected backscatter. These reflected signals, containing tumor backscatter, are spatially focused using a beamformer which compensates for attenuation and phase effects as the signal propagates through the breast. The beamformer generates an energy profile of the breast where high energy regions suggest the presence of breast cancer. Data-Adaptive (DA) beamformers, use an approximation of the desired channel response based on the recorded signal data, as opposed to Data-Independent (DI) algorithms which use an assumed channel model. A novel extension of the DA Robust Capon Beamformer (RCB) is presented in this paper which is shown to significantly outperform existing beamformers, particularly in a dielectrically heterogeneous breast. The algorithm is evaluated on three anatomically accurate electromagnetic (EM) breast models with varying amounts of heterogeneity. The novel beamforming algorithm is compared, using a range of performance metrics, against a number of existing beamformers.

1. INTRODUCTION

Approximately 1.5 million new cases of breast cancer were recorded in the US in 2009 [1], while the estimated mortality rate in Europe was over 1.7 million [2] in 2008. The limitations of the current

de facto breast cancer screening method, X-Ray Mammography, are well documented, particularly when imaging heterogeneously dense breasts [3, 4].

Microwave Imaging is a promising alternative breast imaging modality, which uses backscattered radar signals to identify cancerous regions within the breast [5, 6]. The dielectric contrast between tissue types, notably malignant and normal breast tissues, generate electromagnetic (EM) reflections within the breast. These reflections are recorded and a time-domain image-formation algorithm (beamformer) is applied to determine the location of any dielectric scatterer present. Beamformers can be divided into two distinct categories:

- Data-Independent
- Data-Adaptive

Data-Independent (DI) beamformers use an assumed propagation model to compensate for path dependent attenuation and dispersion [5, 7–12]. Conversely, Data-Adaptive (DA) algorithms process the received signals in order to achieve unit gain from a desired direction, while suppressing signals of the same frequency from all other directions. The signal originating from the desired direction is estimated by varying the weights (via a steering vector) applied to the antenna array [13–17]. This is the basis for the Standard Capon Beamformer (SCB) [13].

The Robust Capon Beamformer (RCB) [14] extends the SCB to more accurately determine the power of the desired waveform, when imprecise knowledge of the antenna array steering vector is available. Guo et al. [15] utilized the RCB algorithm with a monostatic antenna configuration to create a 2D DA microwave energy profile of the breast. Xie et al. [16] further developed the method for a 3D Multistatic Adaptive Microwave Imaging (MAMI) radar system, by implementing the RCB algorithm in two stages (referred to as MAMI 1). The direct application of multistatic data to Guo's RCB adaptation in a single stage was not feasible due to the requirement of excessive computational resources. The MAMI 1 method was extended to incorporate an alternative data-slicing technique (MAMI 2) [17] and both methods were combined under the moniker MAMI C. All of these DA beamforming algorithms were evaluated using relatively homogeneous breast models.

Recently established data on the dielectric properties of the breast [18] has shown that:

- The level of dielectric heterogeneity within the breast had previously been significantly underestimated.

- The dielectric contrast between fibroglandular tissue and cancerous tissue was less than 10%.

These findings illustrate the problems associated with locating cancerous regions within a difficult imaging environment with energy based beamformers [10, 19].

This paper presents a novel extension to the RCB beamforming algorithm, evaluated using a number of anatomically realistic breast models, each with varying levels of dielectric heterogeneity. The proposed algorithm uses a unique signal grouping method, in order to effectively and efficiently apply the RCB method. The performance of this Transmitter Grouping Robust Capon Beamformer (TG-RCB) algorithm is compared against the DI Delay And Sum (DAS) beamformer [5, 7] and DA MAMI C [17] beamforming algorithms.

The remainder of the paper is organized as follows: Section 2 details the TG-RCB algorithm. The numerical breast model model and performance metrics are described in Section 3 and results are presented in Section 4. Finally, conclusions and suggestions for future work are discussed in Section 5.

2. TRANSMITTER GROUPING ROBUST CAPON BEAMFORMER

The proposed algorithm selectively applies the RCB to specific groups of multistatic signals to create a representative energy profile of the breast. First consider a system with M multistatic antenna array elements. For each transmitter, the corresponding M received signals are grouped together and the RCB method is applied to these signals. The resultant waveforms are summed and the focal point energy is calculated across a window. The proposed adaptation is illustrated in Figure 1. This grouping method is significantly different from the original approach taken by Xie et al. [16, 17], where the entire set of M^2 time-aligned multistatic signals are grouped together prior to the application of the RCB algorithm. A RCB algorithm itself is described below for completeness.

For each transmitting element, the received signals are appropriately time aligned [7, 20]. As the received signals may contain errors due to time delay inaccuracies, the RCB is required to approximate a steering vector $\hat{\mathbf{a}}$ and calculate appropriate weights $\hat{\mathbf{w}}_i$. In a group with N time samples, the time-aligned input signals for the i th transmitter are organized as follows:

$$\mathbf{y}_i(t) = [y_1(t), y_2(t), \dots, y_M(t)]^T \quad 0 \leq t \leq (N - 1) \quad (1)$$

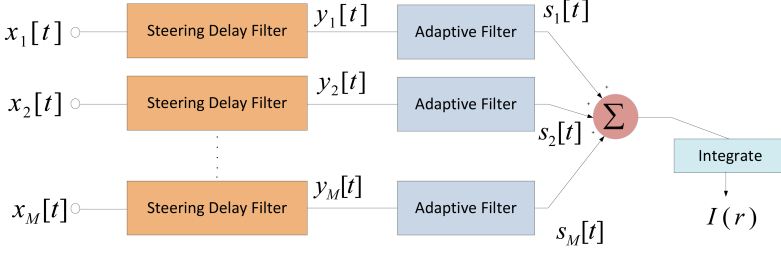


Figure 1. TG-RCB system diagram.

The time delay for the i th transmitting antenna and j th receiving element is calculated as: $\tau_{ij}(\mathbf{r}) = (d_{ij}(\mathbf{r})) / (vT_s)$. The propagation distance between the transmitter (\mathbf{r}_i) to the focal point (\mathbf{r}) and back to the j th receiving antenna location (\mathbf{r}_j) is described as $d_{ij}(\mathbf{r}) = |\mathbf{r} - \mathbf{r}_i| + |\mathbf{r} - \mathbf{r}_j|$. The average speed of signal propagation in breast tissue is denoted by v and T_s is the sampling interval.

The time-aligned input may be modeled as follows:

$$\mathbf{y}_i(t) = \hat{\mathbf{a}}s_i(t) + \mathbf{e}(t) \quad (2)$$

where the scalar $s_i(t)$ denotes the desired backscattered signal, $\hat{\mathbf{a}}$ refers to the array steering vector and \mathbf{e} is a vector containing unwanted noise and interference.

The Robust Capon Beamformer (RCB) problem can be described as:

$$\min_w \hat{\mathbf{w}}^T \hat{\mathbf{R}} \hat{\mathbf{w}} \quad \text{subject to} \quad \hat{\mathbf{w}}^T \hat{\mathbf{a}} = 1 \quad (3)$$

with a solution of:

$$\hat{\mathbf{w}}_i = \frac{\hat{\mathbf{R}}_i^{-1} \hat{\mathbf{a}}}{\hat{\mathbf{a}}^T \hat{\mathbf{R}}_i^{-1} \hat{\mathbf{a}}} \quad (4)$$

with $\hat{\mathbf{w}}_i$ containing the beamformer coefficients and the Sample Covariance Matrix equated as:

$$\hat{\mathbf{R}}_i = \frac{1}{N} \sum_{t=0}^{N-1} \mathbf{y}_i(t) \mathbf{y}_i^T(t) \quad (5)$$

The steering vector $\hat{\mathbf{a}}$ is obtained from the following quadratic problem with associated constraints:

$$\min_a \hat{\mathbf{a}}^T \hat{\mathbf{R}}^{-1} \hat{\mathbf{a}} \quad \|\hat{\mathbf{a}} - \bar{\mathbf{a}}\| \leq \epsilon \quad (6)$$

with $\bar{\mathbf{a}} = (\mathbf{1}_{M \times 1})$ representing an assumed steering vector and ϵ is a user defined variable describing the error in $\hat{\mathbf{a}}$. By applying the weights

to the input vector, the desired backscatter response is calculated as:

$$s_i(t) = \hat{\mathbf{w}}_i^T \cdot \mathbf{y}_i(t) \tag{7}$$

The energy at a specific voxel ($\mathbf{r} = [x, y, z]$) can then be calculated over the window T_{win} as:

$$I(\mathbf{r}) = \int_0^{T_{win}-1} \left[\sum_{i=0}^{M-1} s_i(t) \right]^2 dt \tag{8}$$

3. SIMULATIONS AND METRICS

3.1. Numerical Simulations

Finite Difference Time Domain (FDTD) models of the breast were developed to evaluate the performance of each beamformer. Each FDTD model is based on an MRI-derived breast model, taken from the UWCEM breast phantom repository at the University, of Wisconsin, Madison [21]. In order to adequately evaluate the beamformers, three breast tissue distributions were considered, as shown in Figure 2:

- Homogenous model, comprising of 3 types of adipose tissue (Figures 2(a) and 2(b)).
- Normal model, comprising of 3 types of adipose tissue and a single small scattering of medium fibroglandular tissue (Figures 2(c) and 2(d)).
- Heterogenous model, comprising of all 3 variations of both fibroglandular and adipose tissues (Figures 2(e) and 2(f)).

Table 1. Debye parameters for the FDTD model.

Tissue	ϵ_∞	$(\epsilon_s - \epsilon_{inf})$	σ	t_0
Skin	15.63	8.2	0.82	12.6
Tumor	7	47	0.15	7
Adipose (Low)	2.85	1.10	0.025	13
Fibroglandular (Low)	12.85	24.64	0.251	13
Adipose (Medium)	3.12	1.59	0.050	13
Fibroglandular (Medium)	13.81	35.55	0.738	13
Adipose (High)	3.98	3.54	0.080	13
Fibroglandular (High)	14.28	40.52	0.638	13

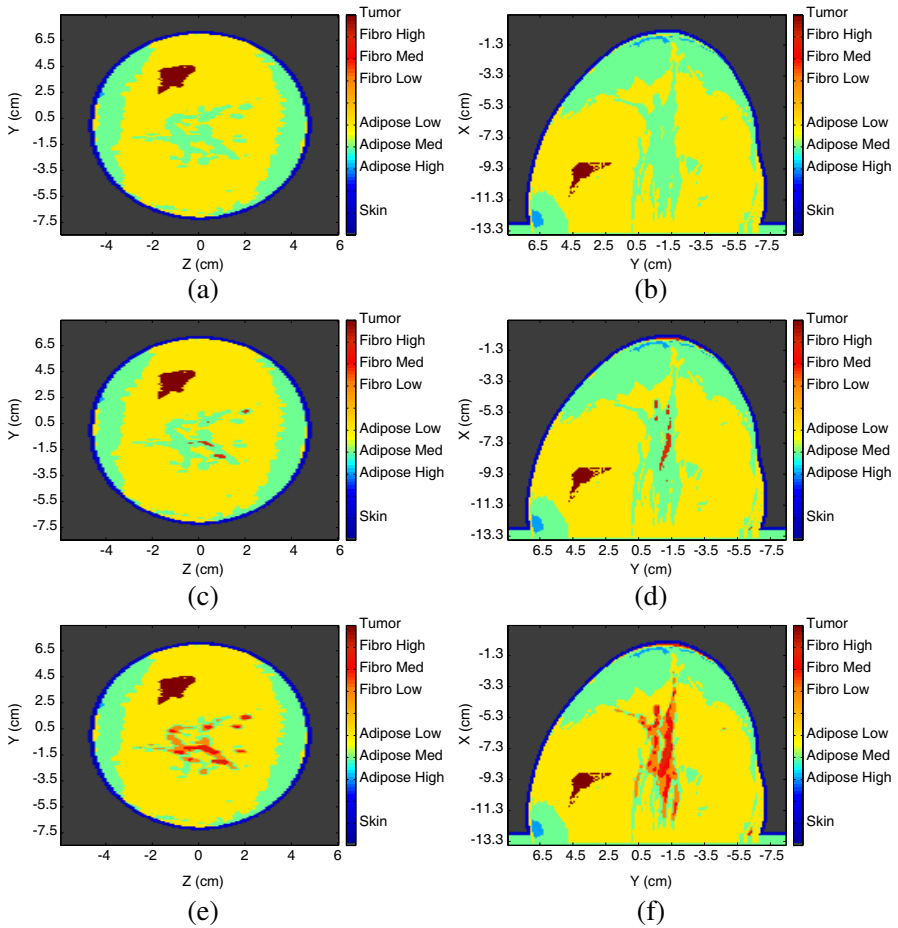


Figure 2. Three breast tissue models with a tumor at $(-9.3, 3.9, -1)$. Slices are taken at $X = -9.3$ cm for Y - Z images and $Z = -1$ cm for X - Y images. (a) and (b) Homogenous model; (c) and (d) Normal model; and (e) and (f) Heterogeneous model.

Dimensions within the 3D region of the breast are described according to each axis. The X axis signifies the depth of the breast, with 0 cm indicating the anterior position. Y and Z represent the span and breadth of the breast respectively, with 0 cm centered at the midpoint of each. A microlobulated tumor (to represent a malignant tumor), is artificially introduced into the FDTD model. Tumors are placed in $(X(\text{cm}), Y(\text{cm}), Z(\text{cm}))$ positions in each simulation, one at $(-9.3, 3.9, -1)$ and another at $(-10.3, -4.7, -1.3)$, corresponding to

Tumors 1 and 2, respectively, in Tables 2, 3 and 4. These tumors are generated using the Gaussian Random Spheres method [22–24] to simulate realistic shapes and surface textures. The variation of tumor size is simulated by modifying the inner sphere radius, resulting in tumors of 5 mm, 10 mm, 15 mm and 20 mm diameters.

The dispersive properties of breast tissue are incorporated into the FDTD model using a single-pole Debye model [25] of the following form:

$$\epsilon_r(\omega) = \epsilon_\infty + \frac{\sigma}{j\omega\epsilon_0} + \frac{(\epsilon_s - \epsilon_\infty)}{1 + j\omega t_0} \tag{9}$$

where ϵ_s is the static permittivity, ϵ_∞ is the permittivity at infinite frequency, ϵ_0 is the permittivity of free space, σ represents the conductivity and t_0 is the relaxation time.

Table 2. Homogenous model results.

Tumor	Radius	SCR (dB)			SMR (dB)			SMXR (dB)		
		DAS	MC	RCB	DAS	MC	RCB	DAS	MC	RCB
1	2.5	21.0	42.6	47.5	14.7	19.1	18.6	9.9	16.0	18.7
	5.0	36.2	57.8	63.2	14.3	16.8	17.1	11.8	13.8	18.0
	7.5	37.2	62.6	66.2	12.8	15.8	15.6	10.9	13.5	21.3
	10.0	42.8	60.9	69.6	11.2	14.4	14.9	11.0	23.6	18.3
2	2.5	29.3	49.3	68.7	15.1	18.4	17.0	12.0	13.5	14.6
	5.0	45.9	64.3	84.9	14.6	17.0	16.5	11.4	11.4	16.3
	7.5	44.7	64.5	87.3	13.6	16.3	16.6	10.8	15.4	15.6
	10.0	42.8	60.6	79.1	11.5	14.7	14.8	10.4	13.6	12.5
AVERAGE		37.5	57.8	70.8	13.5	16.6	16.4	11.0	15.1	16.9

Table 3. Normal model results.

Tumor	Radius	SCR (dB)			SMR (dB)			SMXR (dB)		
		DAS	MC	RCB	DAS	MC	RCB	DAS	MC	RCB
1	2.5	3.1	36.0	58.2	0.8	-0.8	-1.5	-12.7	-15.7	-14.5
	5.0	24.8	40.4	46.1	9.6	12.4	12.4	-1.8	-0.2	-1.0
	7.5	26.7	59.5	55.6	10.4	12.6	13.4	0.7	2.0	3.3
	10.0	28.6	39.5	53.4	10.1	12.1	13.6	3.1	4.6	7.9
2	2.5	6.2	24.2	8.7	3.4	-0.2	3.6	-9.7	-13.4	-10.7
	5.0	18.6	40.3	36.5	11.5	13.2	13.9	0.9	2.9	4.6
	7.5	20.4	41.9	43.1	11.5	12.8	14.9	2.7	4.0	3.6
	10.0	21.9	45.4	43.7	10.7	12.8	14.3	4.4	6.2	8.7
AVERAGE		18.8	40.9	43.2	8.5	9.4	10.6	-1.5	-1.2	0.2

Table 4. Heterogeneous model results.

Tumor	Radius	SCR (dB)			SMR (dB)			SMXR (dB)		
		DAS	MC	RCB	DAS	MC	RCB	DAS	MC	RCB
1	2.5	-0.0	0.1	14.6	-7.3	-6.3	-5.5	-15.0	-13.2	-17.3
	5.0	7.8	12.1	26.8	-1.9	-0.4	3.9	-9.2	-7.4	-7.7
	7.5	10.1	13.6	31.4	0.6	1.7	6.8	-6.6	-4.9	-4.1
	10.0	12.8	16.8	31.6	2.5	3.0	7.9	-4.3	-3.0	-1.4
2	2.5	-0.0	6.6	9.1	-7.8	-4.5	-4.4	-16.3	-12.7	-15.3
	5.0	6.6	8.9	20.2	-2.8	0.1	4.9	-11.1	-7.7	-5.9
	7.5	9.0	12.3	19.0	-0.4	0.9	4.2	-8.6	-6.8	-6.0
	10.0	10.0	9.7	23.1	1.8	0.6	5.9	-6.1	-7.0	-3.0
AVERAGE		7.0	10.0	22.0	-1.9	-0.6	3.0	-9.6	-7.8	-7.6

The dielectric properties for the variations of adipose and fibroglandular tissue are based on the results presented by Zastrow et al. [21]. Skin debye parameters are obtained from published data by Gabriel et al. [26], while debye values representing malignant tissue are taken from Davis et al. [8]. All single pole debye parameters are described in Table 1.

The overall FDTD grid size is approximately 3.3 million cubic cells, the grid resolution is $(1\text{ mm}(dx) \times 1\text{ mm}(dy) \times 1\text{ mm}(dz))$ and the time step dt is defined as $0.833\text{ ps}(dx/2c)$, where c is the speed of light in a vacuum. The FDTD grid is terminated on each side by a 12 layer Universal Perfectly Matched Layer (UPML) [27] in order to minimize edge reflections. In total, 24 FDTD simulations were carried out, based on three distributions of tissue, the two tumor locations and the four tumor diameters.

A cylindrical antenna array [7], consisting of half-wavelength dipole antennas polarized in the direction of the X axis, is placed around the breast. Fifty three antennas are arranged on five rings, as illustrated in Figure 3. The antenna array elements are placed on the skin, with a uniform spacing of 22 mm between each ring along the X axis. The UWB input pulse is a 120 ps differentiated Gaussian pulse, with a center frequency of 7.5 GHz and a -3 dB bandwidth of 9 GHz. An ideal artifact removal algorithm [16] is applied to the backscattered signals to remove the input signal and any reflection from the skin-breast interface. Prior to any signal processing, all FDTD signals are downsampled from 1200 GHz to 50 GHz.

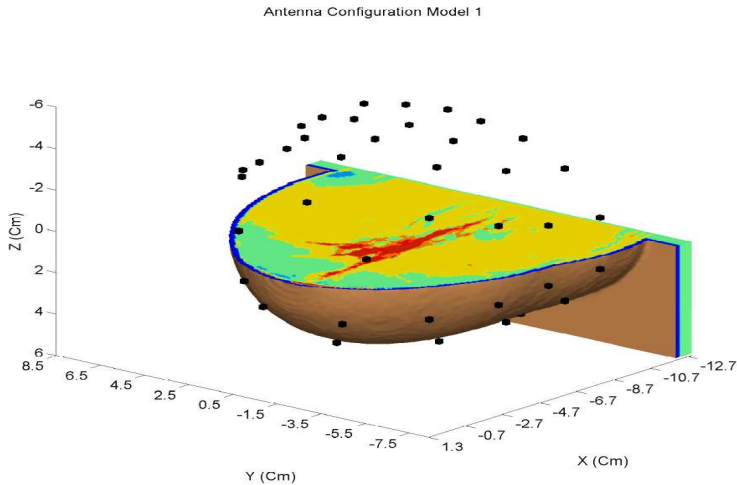


Figure 3. Antenna configuration.

3.2. Metrics

The following metrics are used in order to evaluate each beamformers performance:

- Signal to Clutter ratio (SCR)
- Signal to Mean ratio (SMR)
- Signal to Max ratio (SMXR)

The SMR describes the ratio of the tumor response to the average energy response of all tissue types within the breast [28]. The SCR determines the ratio between the peak tumor response to the maximum clutter energy in the breast [7]. Finally, the SMXR is defined as the ratio of the tumor response to the maximum clutter response in the same breast [28].

4. RESULTS

Resulting images from the beamformer are shown in Figures 4 and 5 as a Y - Z and associated X - Y cross-sectional slice (the tumor location is indicated by a pink circle for clarification in the case of the Normal and Heterogenous tissue models). The TG-RCB algorithm is compared to the DA MAMI-C [17] and DI DAS [5, 7] methods. Furthermore, the corresponding performance metrics (SCR, SMR and SMXR) are shown in Tables 2, 3 and 4. Each table corresponds to a particular level of dielectric heterogeneity.

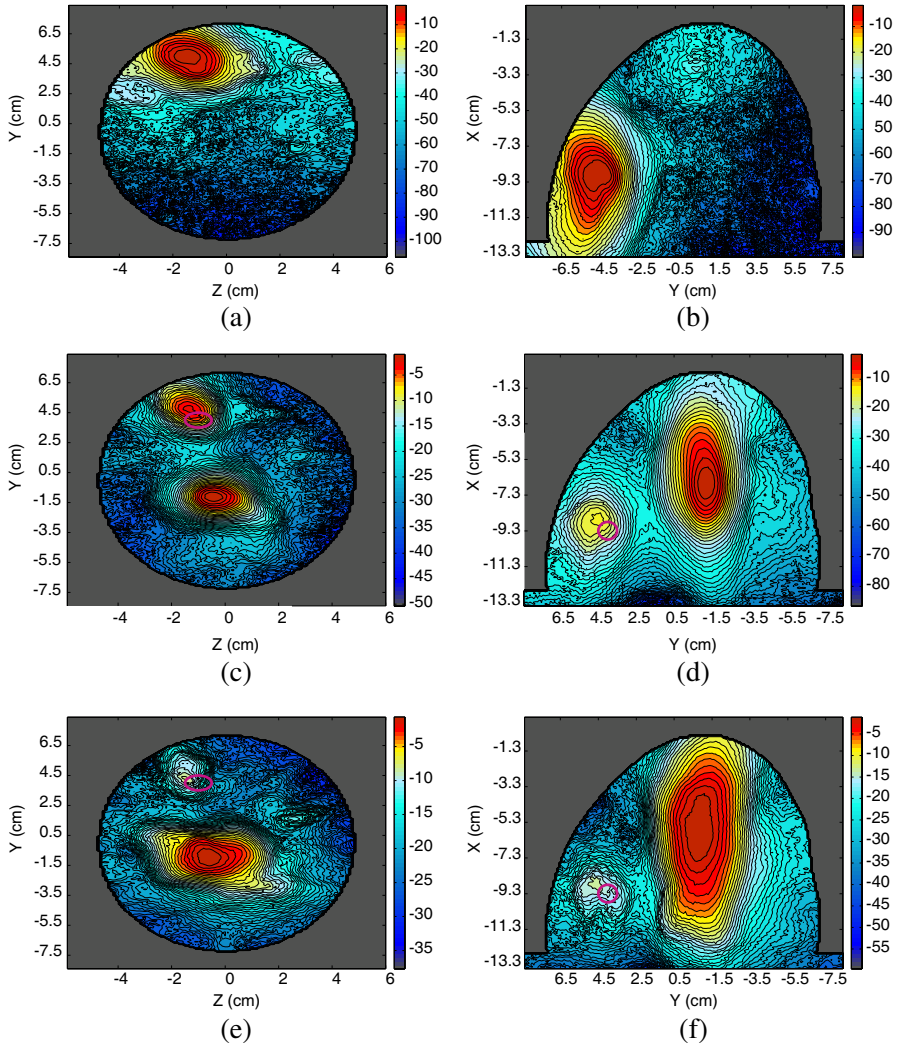


Figure 4. RCB multistatic beamformed images for a tumor located at $(-9.3 \text{ cm}, 3.9 \text{ cm}, -1 \text{ cm})$. Slices are taken at $X = -9.3 \text{ cm}$ for Y - Z images and $Z = -1 \text{ cm}$ for X - Y images. (a) and (b) Homogenous model; (c) and (d) Normal model; and (e) and (f) Heterogeneous model.

Examining the results from the homogeneous model first (Table 2), the TG-RCB algorithm out-performs the DA MAMI C algorithm by an average of 13 dB and 1.8 dB, in terms of SCR and SMXR respectively.

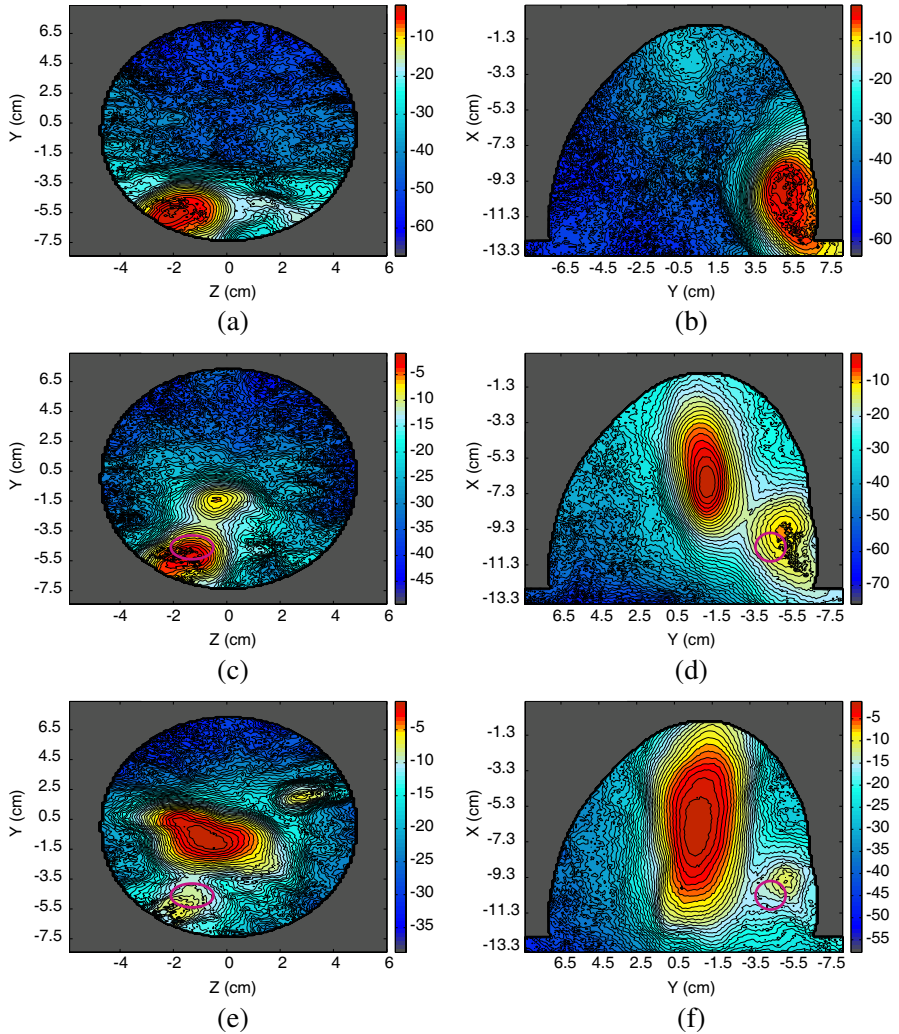


Figure 5. RCB multistatic beamformed images for a tumor located at $(-10.3 \text{ cm}, -4.7 \text{ cm}, -1.3 \text{ cm})$. Slices are taken at $X = -10.3 \text{ cm}$ for Y - Z images and $Z = -1.3 \text{ cm}$ for X - Y images. (a) and (b) Homogenous model. (c) and (d) Normal model. (e) and (f) Heterogeneous model.

Results for SMR between MAMI C and the TG-RCB method are comparable, within 0.2 dB of one another. The DI DAS algorithm is the least effective in this case, where the imaging algorithm averages 33.3 dB, 2.9 dB and 5.9 dB for SCR, SMR and SMXR results. Overall,

the TG-RCB algorithm scores 70.8 dB, 16.4 dB and 16.9 dB in terms of average SCR, SMR and SMXR respectively, for this homogenous breast imaging scenario.

In this basic model, the TG-RCB beamformer performs well, compared to the alternative methods examined. The noise suppression of DA systems have been well documented [14, 15, 17] and in this simple imaging scenario, their improvement over DI systems is clearly evident from the metrics in Table 2. The TG-RCB algorithm significantly reduces clutter in the propagation channel and offers significant improvements over both the DA MAMI C and DI DAS algorithms.

With the presence of a small amount of fibroglandular tissue in the Normal (Table 3) breast model, the TG-RCB algorithm offers improvements of 2.3 dB in SCR, 1.2 dB in SMR and 1 dB in SMXR over its DA counterpart — MAMI C. There is also a significant improvement over the DI DAS method, of 24.4 dB, 2.1 dB and 1.7 dB for SCR, SMR and SMXR respectively. The TG-RCB outperforms all the other imaging methods, scoring an SCR of 43.2 dB, an SMR of 10.6 dB and a SMXR of 0.2 dB.

The performance of all beamforming algorithms degrade with the presence of fibroglandular tissue in the Normal model compared to the Homogenous model, as shown in Table 3. The difference between the assumed and actual propagation channel affects the performance of the each beamformer. The breast can no-longer be considered homogenous, and the contrast between the normal tissue and cancerous tissue is reduced. The results show that the grouping method employed by the TG-RCB algorithm offers superior performance to the MAMI C and DAS algorithms once the breast becomes dielectrically heterogeneous.

The improvement offered by the TG RCB algorithm is further illustrated in the results from the Heterogeneous model (Table 4). The improvement offered by the TG-RCB over MAMI C in terms of SCR, SMR and SMXR is approximately 12 dB, 3.6 dB and 0.2 dB. The DI DAS algorithm is the weakest in this case, trailing the TG-RCB metrics by 15.7 dB, 4.9 dB and 2 dB for SCR, SMR and SMXR respectively. The TG-RCB algorithm is the most effective beamformer when applied to the dielectrically heterogenous breast, achieving an average SCR of 22 dB, SMR of 3 dB and an average SMXR of -7.6 dB.

5. CONCLUSION

In this paper, a novel beamforming approach is proposed for the effective application of the RCB in dielectrically heterogeneous imaging scenarios. The algorithm selects the received signals corresponding

to each transmitter and independently applies the RCB to obtain a desired waveform. The desired waveforms from all transmitting antenna array elements are summed and the energy is calculated across a window. This algorithm was compared to two existing beamforming algorithms, the DAS and MAMI C algorithms. The beamformers were tested on signals obtained from a number of anatomically and dielectrically accurate electromagnetic breast models. For test purposes 24 3D FDTD models were created, with a tumor placed at two different locations within the breast. All beamforming algorithms were examined using three metrics: SCR, SMR and SMXR.

DA beamforming algorithms suppress clutter by minimizing the overall signal power while maintaining the response from the direction of interest. The improved performance of the TG-RCB algorithm within the normal and heterogeneous breast models is evident from the metrics presented here. In a homogeneous breast, containing only one significant dielectric scatterer, the MAMI and TG-RCB beamformer achieve comparable performance, where both offer significant improvements over the DI DAS method. However, in a more dielectrically heterogeneous breast with large amounts of fibroglandular tissue, the tumor is often one of the smaller scatterers present. The MAMI beamformer tends to reward the larger fibrous scatterers, at the expense of the smaller cancerous scatterer. Conversely, the TC-RCB beamformer produces an image where all scatterers present are enhanced in the resultant image, background clutter is suppressed and a dielectrically-representative image is obtained.

Future work will involve using more effective antenna compensation techniques as well as investigating Contrast-Enhanced Imaging with Adaptive beamformers in dielectrically heterogeneous breast models.

REFERENCES

1. Society, A. C., "Cancer facts and figures 2009," American Cancer Society, Tech. Rep., Atlanta, 2009.
2. Ferlay, J., D. Parkin, and E. Steliarova-Foucher, "Estimates of cancer incidence and mortality in europe in 2008," *European Journal of Cancer*, Vol. 46, No. 4, 765–781, 2010.
3. Nass, S. L., I. C. Henderson, and J. C. Lashof, *Mammography and Beyond: Developing Technologies for the Early Detection of Breast Cancer*, National Academy Press, 2001.
4. Huynh, P. H., A. M. Jarolimek, and S. Daye, "The false-negative mammogram," *RadioGraphics*, Vol. 18, 1137–1154, 1998.

5. Hagness, S. C., A. Taflove, and J. E. Bridges, "Two-dimensional fdtd analysis of a pulsed microwave confocal system for breast cancer detection: Fixed focus and antenna array sensors," *IEEE Transactions on Biomedical Engineering*, Vol. 45, 1470–1479, 1998.
6. Meaney, P. M., M. W. Fanning, D. Li, S. P. Poplack, and K. D. Paulsen, "A clinical prototype for active microwave imaging of the breast," *IEEE Transactions on Microwave Theory and Techniques*, Vol. 48, 1841–1853, 2000.
7. Fear, E. C., X. Li, S. C. Hagness, and M. A. Stuchly, "Confocal microwave imaging for breast cancer detection: Localization of tumors in three dimensions," *IEEE Transactions on Biomedical Engineering*, Vol. 47, 812–812, 2002.
8. Davies, S. K., E. J. Bond, X. Li, S. C. Hagness, and B. D. V. Veen, "Microwave imaging via space-time beamforming for the early detection of breast cancer: Beamformer design in the frequency domain," *Journal of Electromagnetic Waves and Applications*, Vol. 17, 357–381, 2003.
9. O'Halloran, M., M. Glavin, and E. Jones, "Performance and robustness of a multistatic mist beamforming algorithm for breast cancer detection," *Progress In Electromagnetics Research*, Vol. 105, 403–424, 2010.
10. Byrne, D., M. O'Halloran, M. Glavin, and E. Jones, "Data independent radar beamforming algorithms for breast cancer detection," *Progress In Electromagnetics Research*, Vol. 107, 331–348, 2010.
11. Lazaro, A., D. Girbau, and R. Villarino, "Wavelet-based breast tumor localization technique using a uwb radar," *Progress In Electromagnetics Research*, Vol. 98, 75–95, 2009.
12. Bindu, G., S. J. Abraham, A. Lonappan, V. Thomas, C. K. Aanandan, and K. T. Mathew, "Active microwave imaging for breast cancer detection," *Progress In Electromagnetics Research*, Vol. 58, 149–169, 2006.
13. Capon, J., "High-resolution frequency-wavenumber spectrum analysis," *Proceedings of the IEEE*, Vol. 57, 1408–1417, 1969.
14. Li, J., P. Stoica, and Z. Wang, "On robust capon beamforming and diagonal loading," *IEEE Transactions on Signal Processing*, Vol. 51, No. 7, 1702–1715, July 2003.
15. Guo, B., Y. Wang, J. Li, P. Stoica, and R. Wu, "Microwave imaging via adaptive beamforming methods for breast cancer detection," *Journal of Electromagnetic Waves and Applications*, Vol. 20, No. 1, 53–63, 2006.

16. Xie, Y., B. Guo, L. Xu, J. Li, and P. Stoica, "Multi-static adaptive microwave imaging for early breast cancer detection," *IEEE Transactions on Biomedical Engineering*, Vol. 53, 1647–1657, 2006.
17. Xie, Y., B. Guo, J. Li, and P. Stoica, "Novel multistatic adaptive microwave imaging methods for early breast cancer detection," *EURASIP Journal on Applied Signal Processing*, Vol. 2006, 1–13, 2006.
18. Lazebnik, M., L. McCartney, D. Popovic, C. B. Watkins, M. J. Lindstrom, J. Harter, S. Sewall, A. Magliocco, J. H. Booske, M. Okoniewski, and S. C. Hagness, "A large-scale study of the ultrawideband microwave dielectric properties of normal breast tissue obtained from reduction surgeries," *Physics in Medicine and Biology*, Vol. 52, 2637–2656, 2007.
19. O'Halloran, M., M. Glavin, and E. Jones, "Effects of fibroglandular tissue distribution on data-independent beamforming algorithms," *Progress In Electromagnetics Research*, Vol. 97, 141–158, 2009.
20. Li, X. and S. C. Hagness, "A confocal microwave imaging algorithm for breast cancer detection," *IEEE Microwave and Wireless Communications Letters*, Vol. 11, 130–132, 2001.
21. Zastrow, E., S. K. Davis, M. Lazebnik, F. Kelcz, B. D. V. Veen, and S. Hagness, "Development of anatomically realistic numerical breast phantoms with accurate dielectric properties for modeling microwave interactions with the human breast," *IEEE Transactions on Biomedical Engineering*, Vol. 55, No. 12, 2792–2800, Dec. 2008.
22. Muinonen, K., "Introducing the gaussian shape hypothesis for asteroids and comets," *Astronomy and Astrophysics*, Vol. 332, 1087–1098, 1998.
23. Conceicao, R. C., M. O'Halloran, M. Glavin, and E. Jones, "Support vector machines for the classification of early-stage breast cancer based on radar target signatures," *Progress In Electromagnetics Research B*, Vol. 23, 311–327, 2010.
24. Conceicao, R. C., M. O'Halloran, E. Jones, and M. Glavin, "Investigation of classifiers for early-stage breast cancer based on radar target signatures," *Progress In Electromagnetics Research*, Vol. 105, 295–311, 2010.
25. Okoniewski, M., M. Mrozowski, and M. A. Stuchly, "Simple treatment of multi-term dispersion in fdtd," *IEEE Microwave and Guided Wave Letters*, Vol. 7, 121–123, 1997.
26. Gabriel, C., S. Gabriel, and E. Corthout, "The dielectric

- properties of biological tissues: I. Literature survey,” *Phys. Med. Biol.*, Vol. 41, No. 11, 2231–2249, Nov. 1996.
27. Berenger, J. P., “A perfectly matched layer for the absorption of electromagnetic waves,” *Journal of Computational Physics*, Vol. 114, 185–200, 1994.
 28. Conceicao, R., M. O’Halloran, M. Glavin, and E. Jones, “Comparison of planar and circular antenna configurations for breast cancer detection using microwave imaging,” *Progress In Electromagnetics Research*, Vol. 99, 1–19, 2009.